Dalton Transactions

PAPER

View Article Online
View Journal | View Issue

Cite this: *Dalton Trans.*, 2015, **44**, 6229

The first example of Tb_3-containing metallopolymer-type hybrid materials with efficient and high color-purity green luminescence†

Zhao Zhang,[a] Heini Feng,[a] Lin Liu,[a] Chao Yu,[a] Xingqiang Lü,*[a] Xunjin Zhu,[b] Wai-Kwok Wong,[b] Richard A. Jones,[c] Mei Pan[d] and Chengyong Su*[d]

Received 12th January 2015,
Accepted 16th February 2015

DOI: 10.1039/c5dt00141b

www.rsc.org/dalton

In the series of homo-leptic trinuclear complexes {[$Ln_3(L)_4Cl_4(MeOH)(H_2O)$]·Cl} (Ln = La, **1**; Ln = Eu, **2**; Ln = Tb, **3** or Ln = Gd, **4**) self-assembled from the allyl-modified benzimidazole-type ligand **HL** (4-allyl-2-(1*H*-benzo[*d*]imidazol-2-yl)-6-methoxyphenol) and $LnCl_3·6H_2O$, a suitable energy level match endows efficient green luminescence ($\Phi_{overall}$ = 72%) of Tb_3-arrayed complex **3**. The copolymerization between each of these complex monomers **1–4** and C=C-containing MMA (methyl methacrylate) or NBE (norbornene) shows that degradative chain transfer of the terminal four flexible allyl groups within restrains their radical polymerization with MMA while it does not hinder their effective ring-opening metathesis polymerization (ROMP) with NBE. Thus, two kinds of PMMA-supported doping hybrid materials **1@PMMA**, **2@PMMA**, **3@PMMA** and **4@PMMA** and PNBE-supported metallopolymer-type hybrid materials **Poly-(NBE-1)**, **Poly(NBE-2)**, **Poly(NBE-3)** and **Poly(NBE-4)** are obtained, respectively. Especially for both **3@PMMA** and **Poly(NBE-3)** with high color-purity characteristic green emission of Tb^{3+} ions, improved physical properties including significantly enhanced luminescence ($\Phi_{overall}$ = 76% or 83%) are observed, and covalent-bonding endows a higher-concentration self-quenching as compared to physical doping.

1. Introduction

Due to the large Stokes shift, the ms-grade long lifetime and the characteristic narrow line-like emission of Eu^{3+} or Tb^{3+} ions, there has been growing interest in the development of new kinds of high color-purity Eu^{3+}- (red) or Tb^{3+}-based (green) optical materials with potential applications in organic light-emitting diodes (OLEDs),[1] white light-emitting devices,[2] color-tuning pigments[3] or a biological fluoro-immunoassay.[4] However, limited by the forbidden parity from f–f transitions of these two inorganic Ln^{3+} ions, the molar absorption coefficients are normally very low (ε = 0.01–10 M^{-1} cm^{-1}). From the viewpoint of effective sensitization, a suitable chromophore is required to allow for indirect population of those Ln^{3+} ions' emissive excited states through ligand excitation ("antenna effect").[5] For this purpose, compatibility between the excited state level of the chromophore and the accepting level of the corresponding Ln^{3+} ion should be realized[6] in these luminescent Ln^{3+}-complexes besides the avoidance of the non-radiative deactivation by OH-, NH- or CH-oscillators around the Ln^{3+} ion.[7] Nevertheless, the Ln^{3+}-complexes generally present low thermal stability and poor mechanical properties, giving rise to another parallel challenge.

[a]*School of Chemical Engineering, Shaanxi Key Laboratory of Degradable Medical Material, Northwest University, Xi'an 710069, Shaanxi, P. R. China. E-mail: lvxq@nwu.edu.cn; Tel: +86-29-88302312(o)*

[b]*Department of Chemistry, Hong Kong Baptist University, Waterloo Road, Kowloon Tong, Hong Kong, P. R. China*

[c]*Department of Chemistry and Biochemistry, The University of Texas at Austin, 1 University Station A5300, Austin, TX 78712-0165, USA*

[d]*MOE Laboratory of Bioinorganic and Synthetic Chemistry/KLGH EI of Environment and Energy Chemistry, School of Chemistry and Chemical Engineering, Sun Yat-Sen University, Guangzhou 510275, Guangdong, China. E-mail: cesscy@mail.sysu.edu.cn; Tel: +86-20-84115178(o)*

†Electronic supplementary information (ESI) available: The synthesis and characterization of **PMMA** in activation with AIBN and **PNBE** in activation with H–Grubbs II in ESI; the selected bond lengths (Å) and bond angles (°) for **3**·2MeOH·$4H_2O$ and GPC data of the samples of **PMMA**, **PNBE** and the series of metallopolymers **Poly(NBE-1)**, **Poly(NBE-2)**, **Poly(NBE-3)** and **Poly(NBE-4)** in Tables 1 and 2S; perspective drawing of the weak N1–H1···Cl5 H-bonding (3.045 (2) Å) interaction between the host framework and the free Cl5 in complex **3**·2MeOH·$4H_2O$ and the visible emission and excitation spectra of complex **4** in MeCN solution at 1 × 10^{-5} M and the hybrid materials **4@PMMA** and **Poly-(NBE-4)** with the feeding molar ratio of 400 : 1 in the solid state at 77 K in Fig. 1 and 2S, respectively. CCDC 1035177. For ESI and crystallographic data in CIF or other electronic format see DOI: 10.1039/c5dt00141b

In order to overcome these deficiencies and simultaneously improve the photo-physical properties of these Ln^{3+}-complexes, one of the simple but effective solutions is physical doping into a host inorganic or organic polymeric matrix.[8] On the other hand, an alternative approach is to trap the Ln^{3+}-complex into a silica-based host[9] or a polymer backbone[10] with covalent bonds for the formation of grafting-type inorganic–organic hybrid materials. By contrast, Ln^{3+}-containing metallopolymers,[11] as a unique class of grafted hybrid materials, possess both the beneficial properties of inorganic Ln^{3+} ions and the attractive features of organic polymers, including mechanical strength, flexibility, ease of processing and low cost. This advantage, especially when compared with Ln^{3+}-containing doping hybrid materials, endows the ability to effectively resolve the high homogeneity and clustering of emitters and makes them more ideal as optoelectronic materials. So far, to the best of our knowledge, the developed Ln^{3+}-containing metallopolymers are usually limited from the mononuclear Ln^{3+}-complexes through coupling,[12] ring-opening polymerization,[13] radical polymerization[14] or electropolymerization,[15] and few systems have been fabricated from d–f heterometallic[16] or f–f polymetallic complexes.[17] In our recent reports, through the radical copolymerization of the divinyl-modified ZnLn or Zn_2Ln (Ln = Nd, Yb or Er) Salen-type Schiff-base complex monomer and another C=C-containing monomer, two examples of near-infrared (NIR) luminescent ZnLn[16b,c] or Zn_2Ln-containing[16d] metallopolymers were constructed. Moreover, another example of NIR luminescent metallopolymers based on allyl-modified $Ln_4(Salen)_4$ (Ln = Nd or Yb) complexes was successfully built by controlled ring-opening metathesis polymerization (ROMP) with norbornene (NBE).[17] In the two kinds of metallopolymers, additive electronic communication between the homo- or hetero-multiple metal centers actually induces more efficient energy transfer. Considering the relatively higher first excited state (17 286 cm^{-1}, $^5D_0$ for Eu^{3+}; 20 545 cm^{-1}, $^5D_4$ for Tb^{3+}) of visible luminescent Eu^{3+} or Tb^{3+} ions than that (11 257 cm^{-1}, $^4F_{3/2}$ for Nd^{3+}; 10 400 cm^{-1}, $^2F_{5/2}$ for Yb^{3+}, 6610 cm^{-1}, $^4I_{13/2}$ for Er^{3+}) of NIR luminescent Nd^{3+}, Yb^{3+} or Er^{3+} ions,[18] new organic ligands also with unsaturated C=C functions and not vinyl- or allyl-modified Salen-type Schiff-base ligands need to be designed, where the polymerizable multi-metallic Eu^{3+} or Tb^{3+} complex monomer with higher $^3\pi$–π^* energy level that matched well with the first excited state of Eu^{3+} or Tb^{3+} ions can also be copolymerized with other C=C-containing monomers. Thus, new polymetallic-containing metallopolymers with Eu^{3+}- or Tb^{3+}-based high color-purity visible emission are expected. Herein, by the self-assembly of the allyl-modified benzimidazole-type ligand **HL** and $LnCl_3{\cdot}6H_2O$ (Ln = La, Eu, Tb or Gd), a series of homo-leptic trinuclear complexes $\{[Ln_3(L)_4Cl_4(MeOH)(H_2O)]{\cdot}Cl\}$ (Ln = La, **1**; Ln = Eu, **2**; Ln = Tb, **3** or Ln = Gd, **4**) are obtained, respectively. The series of Ln_3-arrayed (Ln = Eu or Tb) complex monomers with four terminal allyl groups should be copolymerized with MMA or NBE, and thus, the first example of high color-purity Eu^{3+}- or Tb^{3+}-based trimetallic emissive metallopolymers could be anticipated.

2. Experimental

Materials and methods

High performance liquid chromatography (HPLC) grade tetrahydrofuran (THF) was purchased from Fisher Scientific and purified over solvent columns. Other solvents were used as received from Sigma Aldrich and stored over 3 Å activated molecule sieves. Methyl methacrylate (MMA) was dried over CaH_2, distilled and stored under dry N_2 prior to use. Azobis-(isobutyronitrile) (AIBN) was purified by recrystallization twice from absolute MeOH prior to use. Other chemicals containing Hoveyda–Grubbs II (H–Grubbs II) and norbornene (NBE) were commercial products of reagent grade and were used without further purification. All manipulations of air and water sensitive compounds were carried out under dry N_2 using standard Schlenk line techniques. Elemental analyses were performed using a Perkin-Elmer 240C elemental analyzer. Infrared spectra were recorded using a Nicolet Nagna-IR 550 spectrophotometer in the region 4000–400 cm^{-1} using KBr pellets. ^1H NMR spectra were recorded using a JEOL EX 400 spectrometer with $SiMe_4$ as the internal standard in CD_3CN, $CDCl_3$ and/or DMSO-δ_6 at room temperature. ESI-MS was performed using a Finnigan LCQ^{DECA} XP HPLC-MS_n mass spectrometer with a mass to charge (m/z) range of 4000 using a standard electrospray ion source and MeCN as a solvent. Electronic absorption spectra in the UV/Visible region and diffuse reflection (DR) spectra were recorded with a Cary 300 UV spectrophotometer, steady-state visible fluorescence and PL excitation spectra were recorded using a Photon Technology International (PTI) Alpha scan spectrofluorometer, and visible decay spectra were recorded using a pico-N_2 laser system (PTI Time Master). The quantum yield ($\Phi_{overall}$) of visible luminescence for each sample in solution was determined by the relative comparison procedure, using a reference of a known quantum yield (quinine sulfate in dilute H_2SO_4 solution, Φ_r = 0.546). The quantum yield ($\Phi_{overall}$) of visible luminescence for each solid state sample was determined by the absolute method using an integrating sphere[19] (150 nm diameter, $BaSO_4$ coating) on an Edinburgh Instrument FLS928. Three parallel measurements were carried out for each sample, so that the presented $\Phi_{overall}$ value corresponds to the arithmetic mean value with the estimated error of 10%. Gel permeation chromatography (GPC) analyses of the polymers were performed using a Waters 1525 binary pump coupled to a Waters 2414 refractive index detector with HPLC THF as the eluent on American Polymer Standard 10 μm particle size, linear mixed bed packing columns. The GPC was calibrated using polystyrene standards. The powder X-ray diffraction (PXRD) patterns were recorded using a D/Max-IIIA diffractometer with graphite-monochromatized Cu Kα radiation (λ = 1.5418 Å). Thermogravimetric (TG) analyses were carried out using a NETZSCH TG 209 instrument under flowing nitrogen by heating the samples from 25 to 600 °C.

Synthesis of 5-allyl-2-hydroxy-3-methoxy-benzaldehyde

5-Allyl-2-hydroxy-3-methoxy-benzaldehyde was obtained by the Williamson synthesis from *o*-vanillin (6.08 g, 40 mmol) and

allyl bromide (12.0 mL, 140 mmol) as the starting materials in the presence of anhydrous K_2CO_3 (11.06 g, 80 mmol) and the subsequent *para* Claisen rearrangement according to a well-established procedure from the literature.[17] Yield: 3.92 g, 51%. Element analysis (%): calcd for $C_{11}H_{12}O_3$ (192.21): C, 68.74; H, 6.29. Found: C, 68.72; H, 6.34. ^{1}H NMR (400 MHz, $CDCl_3$): δ (ppm) 11.10 (s, 1H, –OH), 9.90 (s, 1H, –CHO), 6.99 (s, 1H, –Ph), 6.95 (s, 1H, –Ph), 5.97 (m, 1H, –CH═C), 5.13 (m, 2H, ═CH_2), 3.91 (s, 3H, –OMe), 3.38 (s, 2H, –CH_2).

Synthesis of the diallyl-modified Salen-type Schiff-base precursor H_2L^0 (H_2L^0 = *N*,*N*′-bis(5-allyl-3-methoxy-salicylidene)-phenylene-1,2-diamine)

To a stirred solution of *o*-phenylenediamine (0.55 g, 5 mmol) in absolute EtOH (20 mL), 5-allyl-2-hydroxy-3-methoxy-benzaldehyde (1.92 g, 10 mmol) was added, and the resulting mixture was continuously stirred under an N_2 atmosphere at room temperature for 12 h. The insoluble red precipitate was filtered and washed with cold diethyl ether to give a red polycrystalline solid. Yield: 1.46 g, 64%. Element analysis (%): calcd for $C_{28}H_{28}N_2O_4$ (456.64): C, 73.66; H, 6.18; N, 6.14. Found: C, 73.75; H, 6.15; N, 6.06. FT-IR (KBr, cm^{-1}): 3320 (b), 3070 (w), 2993 (w), 2943 (w), 2898 (w), 2839 (w), 1620 (s), 1581 (m), 1475 (s), 1394 (m), 1344 (w), 1267 (vs), 1230 (w), 1209 (w), 1161 (m), 993 (s), 966 (w), 908 (m), 840 (w), 800 (w), 746 (w), 686 (w), 600 (w), 545 (w), 503 (w), 480 (w). ^{1}H NMR (400 MHz, CD_3CN): δ (ppm) 13.16 (s, 2H, –OH), 8.71 (s, 2H, –CH═N), 7.37 (m, 4H, –Ph), 6.94 (s, 4H, –Ph), 6.01 (m, 2H, –CH═C), 5.10 (m, 4H, ═CH_2), 3.86 (s, 6H, –OMe), 3.36 (m, 4H, –CH_2).

Synthesis of the allyl-modified benzimidazole-type ligand HL (HL = 4-allyl-2-(1*H*-benzo[*d*]imidazol-2-yl)-6-methoxyphenol)

The solution of the diallyl-modified Salen-type Schiff-base precursor $\mathbf{H_2L^0}$ (4.56 g, 10 mmol) in absolute MeOH (20 mL) was refluxed under an N_2 atmosphere for 36 h, where the color of the solution changed from dark red to brown and white. After cooling to room temperature, the volatile materials were removed under vacuum, and the colorless solid residue (**HL**) that remained was washed with absolute EtOH and dried under vacuum. Yield: 1.96 g, 70%. Element analysis (%): calcd for $C_{17}H_{16}N_2O_2$ (280.33): C, 72.84; H, 5.75; N, 9.99. Found: C, 72.76; H, 5.87; N, 9.91. FT-IR (KBr, cm^{-1}): 3651 (w), 3524 (w), 3464 (w), 3067 (w), 2970 (w), 2928 (w), 2907 (w), 2837 (w), 2766 (w), 2731 (w), 2654 (w), 2596 (w), 2531 (w), 2486 (w), 2293 (w), 2259 (w), 2212 (w), 2116 (w), 2021 (w), 1977 (w), 1933 (w), 1894 (w), 1846 (w), 1827 (w), 1776 (w), 1722 (w), 1624 (s), 1599 (m), 1499 (s), 1454 (s), 1398 (s), 1342 (w), 1254 (vs), 1146 (s), 1063 (s), 997 (s), 964 (w), 914 (m), 851 (m), 800 (m), 748 (m), 681 (w), 615 (m), 548 (w), 494 (w), 434 (w). ^{1}H NMR (400 MHz, CD_3CN): δ (ppm) 12.99 (s, 1H, –NH), 11.09 (s, 1H, –OH), 7.72 (d, 1H, –Ph), 7.60 (d, 1H, –Ph), 7.31 (m, 3H, –Ph), 6.94 (s, 1H, –Ph), 6.09 (m, 1H, –CH═C), 5.17 (m, 2H, ═CH_2), 3.90 (s, 3H, –OMe), 3.44 (d, 2H, –CH_2).

Synthesis of homo-leptic trinuclear complexes {$[Ln_3(L)_4Cl_4(MeOH)(H_2O)]\cdot Cl$} (Ln = La, 1; Ln = Eu, 2; Ln = Tb, 3 or Ln = Gd, 4)

A CH_2Cl_2–MeOH solution (10 mL, v/v = 1 : 1) containing **HL** (168 mg, 0.6 mmol) and Et_3N (84 μL, 0.6 mmol) was stirred for 30 min at RT, then a solution of $LnCl_3\cdot 6H_2O$ (0.6 mmol, Ln = La, 212 mg; Ln = Eu, 220 mg; Ln = Tb, 224 mg or Ln = Gd, 223 mg) in absolute MeOH (5 mL) was added and the mixture was refluxed under an N_2 atmosphere for 3 h, respectively. After cooling to RT, the resulting respective clear yellow solution was filtered, and diethyl ether was allowed to diffuse slowly into the filtrate at RT. Pale yellow microcrystalline products were obtained in about two weeks, respectively.

For **1**: yield: 193 mg, 73%. Element analysis (%): calcd for $C_{69}H_{66}N_8O_{10}Cl_5La_3$ (1761.31): C, 47.05; H, 3.78; N, 6.36. Found: C, 47.15; H, 3.94; N, 6.28. FT-IR (KBr, cm^{-1}): 3380 (b), 3220 (s), 2977 (s), 2940 (s), 2740 (m), 2679 (s), 2491 (w), 1620 (s), 1570 (s), 1507 (vs), 1465 (s), 1430 (s), 1399 (m), 1351 (m), 1276 (m), 1246 (s), 1211 (m), 1171 (w), 1133 (m), 1057 (s), 1039 (w), 1010 (w), 994 (s), 917 (w), 851 (m), 820 (w), 770 (s), 748 (s), 683 (w), 654 (w), 623 (w), 585 (w), 569 (w), 530 (w), 498 (w). ^{1}H NMR (400 MHz, DMSO-d_6): δ (ppm) 13.17 (s, 4H, –NH), 8.24 (m, 1H, –OH), 7.79 (m, 2H, –Ph), 7.71 (m, 4H, –Ph), 7.61 (m, 2H, –Ph), 7.49 (m, 4H, –Ph), 7.39 (m, 3H, –Ph), 7.27 (m, 3H, –Ph), 7.18 (m, 6H, –Ph), 6.03 (m, 4H, –CH═C), 5.13 (m, 8H, ═CH_2), 3.87 (s, 3H, MeOH), 3.83 (s, 12H, –OMe), 3.33 (s, 8H, –CH_2). ESI-MS (in MeCN) *m*/*z*: 1725.86 (100%), $[M - Cl]^+$; 1762.32 (18%), $[M + H]^+$.

For **2**: yield: 192 mg, 71%. Element analysis (%): calcd for $C_{69}H_{66}N_8O_{10}Cl_5Eu_3$ (1800.48): C, 46.03; H, 3.69; N, 6.22. Found: C, 46.06; H, 3.82; N, 6.15. FT-IR (KBr, cm^{-1}): 3373 (b), 3210 (m), 2945 (m), 2841 (m), 1622 (s), 1571 (s), 1522 (m), 1487 (vs), 1463 (s), 1445 (s), 1424 (s), 1345 (m), 1307 (w), 1280 (m), 1243 (s), 1202 (m), 1140 (m), 1057 (s), 1012 (w), 1000 (s), 957 (w), 910 (m), 865 (w), 850 (w), 817 (m), 766 (s), 748 (s), 686 (w), 654 (w), 624 (w), 574 (w), 499 (w). ESI-MS (in MeCN) *m*/*z*: 1765.02 (100%), $[M - Cl]^+$; 1801.48 (16%), $[M + H]^+$.

For **3**: yield: 189 mg, 69%. Element analysis (%): calcd for $C_{69}H_{66}N_8O_{10}Cl_5Tb_3$ (1821.37): C, 45.50; H, 3.65; N, 6.15. Found: C, 45.47; H, 3.74; N, 6.10. FT-IR (KBr, cm^{-1}): 3390 (b), 3227 (m), 2975 (m), 2941 (m), 2737 (m), 2677 (m), 2490 (w), 1621 (s), 1570 (s), 1507 (s), 1495 (vs), 1464 (s), 1431 (m), 1398 (m), 1350 (w), 1278 (w), 1245 (s), 1211 (w), 1171 (w), 1133 (w), 1057 (m), 1037 (w), 995 (s), 917 (w), 825 (w), 821 (w), 770 (s), 747 (m), 688 (w), 655 (w), 623 (w), 589 (w), 502 (w). ESI-MS (in MeCN) *m*/*z*: 1785.92 (100%), $[M - Cl]^+$; 1822.38 (13%), $[M + H]^+$.

For **4**: yield: 185 mg, 68%. Element analysis (%): calcd for $C_{69}H_{66}N_8O_{10}Cl_5Gd_3$ (1816.35): C, 45.63; H, 3.66; N, 6.17. Found: C, 45.97; H, 3.81; N, 6.08. FT-IR (KBr, cm^{-1}): 3378 (b), 3219 (m), 2977 (m), 2941 (m), 2739 (m), 2679 (m), 2492 (w), 1620 (s), 1571 (s), 1507 (s), 1465 (vs), 1434 (s), 1399 (m), 1352 (m), 1278 (m), 1246 (s), 1211 (m), 1170 (w), 1133 (m), 1057 (s), 1037 (w), 1010 (w), 995 (s), 917 (w), 852 (m), 820 (w), 771 (s), 748 (s), 687 (w), 654 (w), 623 (w), 589 (w), 569 (w),

531 (w), 499 (w). ESI-MS (in MeCN) m/z: 1780.89 (100%), $[M - Cl]^+$; 1817.35 (14%), $[M + H]^+$.

Determination of the crystal structure

Single crystals for **3**·2MeOH·4H_2O of suitable dimensions were mounted onto thin glass fibers. All the intensity data were collected using a Bruker SMART CCD diffractometer (Mo-Kα radiation and λ = 0.71073 Å) in Φ and ω scan modes. Structures were solved by direct methods followed by difference Fourier syntheses, and then refined by full-matrix least-squares techniques against F^2 using SHELXTL.[20] All other non-hydrogen atoms were refined with anisotropic thermal parameters. Absorption corrections were applied using SADABS.[21] All hydrogen atoms were placed in calculated positions and refined isotropically using a riding model. Crystallographic data and refinement parameters for the complexes are presented in Table 1. Relevant atomic distances and bond angles are collected in Table 1S.† CCDC reference number 1035177 is for **3**·2MeOH·4H_2O.

Synthesis of PMMA-supported doping hybrid materials 1@PMMA, 2@PMMA, 3@PMMA and 4@PMMA

The homogeneous polymerization of MMA and each of the complexes {[Ln_3(L)$_4Cl_4$(MeOH)(H_2O)]·Cl} (Ln = La, **1**; Ln = Eu, **2**; Ln = Tb, **3** or Ln = Gd, **4**) with a stipulated feeding molar ratio (200 : 1, 400 : 1, 600 : 1 or 800 : 1) in activation with AIBN was carried out in a Fisher-Porter glass reactor and protected by dry N_2 according to the typical procedure.[22] A mixture of MMA (2.7 mL, 25.3 mmol) in activation with AIBN (37.6 mg, 1.5 mol% of MMA) and {[Ln_3(L)$_4Cl_4$(MeOH)(H_2O)]·Cl} (0.063 mmol; Ln = La (**1**), 111 mg; Ln = Eu (**2**), 114 mg; Ln = Tb (**3**), 115 mg or Ln = Gd (**4**), 116 mg) was dissolved in dry xylene (30 mL), and the resulting homogeneous solution was purged with N_2 for 10 min and sealed under a reduced N_2 atmosphere. The solution was heated to 60 °C with continuous stirring for 24 h. The viscous mixture was diluted with dry THF (20 mL) and precipitated with absolute diethyl ether (50 mL) three times. The resulting solid products were collected by filtration and dried at 45 °C under vacuum to a constant weight, respectively.

Table 1 Crystal data and structure refinement for complex **3**·2MeOH·4H_2O

Compound	**3**·2MeOH·4H_2O
Empirical formula	$C_{71}H_{82}Cl_5N_8O_{16}Tb_3$
Formula weight	1957.46
Crystal size/mm	0.26 × 0.23 × 0.21
T/K	296(2)
λ/Å	0.71073
Crystal system	Triclinic
Space group	$P\bar{1}$
a/Å	16.089(15)
b/Å	17.155(17)
c/Å	18.684(17)
α/°	71.523(16)
β/°	80.787(19)
γ/°	62.199(15)
V/Å^3	4326(7)
Z	2
ρ/g cm^{-3}	1.503
μ/mm^{-1}	2.641
F(000)	1944
Data/restraints/parameters	15 042/53/908
Quality-of-fit indicator	0.976
Final R indices [$I > 2\sigma(I)$]	R_1 = 0.0975 wR_2 = 0.2480
R indices (all data)	R_1 = 0.1798 wR_2 = 0.3223

For **1@PMMA** (400 : 1): yield: 91%. FT-IR (KBr, cm^{-1}): 3631 (w), 3381 (m), 3221 (w), 3300 (w), 2996 (m), 2949 (m), 2844 (w), 1732 (vs), 1625 (m), 1570 (w), 1505 (w), 1460 (m), 1390 (s), 1348 (w), 1309 (w), 1255 (w), 1201 (w), 1058 (w), 1045 (w), 1018 (w), 1002 (w), 960 (w), 867 (w), 823 (w), 767 (m), 746 (m), 684 (w), 658 (w), 585 (w), 555 (w), 514 (w), 466 (w). ^{1}H NMR (400 MHz, DMSO-δ_6–$CDCl_3$, v/v = 10 : 1): δ (ppm) 13.12 (s, 4H, –NH), 8.20 (m, 1H, –OH), 7.78 (m, 2H, –Ph), 7.70 (m, 4H, –Ph), 7.61 (m, 2H, –Ph), 7.48 (m, 4H, –Ph), 7.38 (m, 3H, –Ph), 7.27 (m, 3H, –Ph), 7.17 (m, 6H, –Ph), 6.01 (m, 4H, –CH═C), 5.11 (m, 8H, ═CH_2), 3.86 (s, 3H, MeOH), 3.83 (s, 12H, –OMe), 3.56 (s, 330H, –COOMe), 3.32 (s, 8H, –CH_2), 1.85 (b, 220H, –CH_2), 0.91 (m, 330H, –CH_3).

For **2@PMMA** (400 : 1): yield: 90%. FT-IR (KBr, cm^{-1}): 3624 (w), 3383 (m), 3219 (w), 3301 (w), 3070 (w), 2996 (m), 2950 (m), 2841 (w), 1731 (vs), 1624 (m), 1570 (w), 1501 (w), 1466 (w), 1391 (s), 1345 (w), 1308 (w), 1252 (w), 1200 (w), 1059 (w), 1041 (w), 1017 (w), 1000 (w), 966 (w), 868 (w), 820 (w), 765 (m), 746 (m), 681 (w), 650 (w), 580 (w), 551 (w), 510 (w), 461 (w).

For **3@PMMA** (200 : 1, 400 : 1, 600 : 1 and 800 : 1): yield: 83% (200 : 1); 89% (400 : 1); 91% (600 : 1); 92% (800 : 1). FT-IR (KBr, cm^{-1}): 3620 (w), 3379 (m), 3222 (w), 3301 (w), 2998 (m), 2948 (m), 2841 (w), 1731 (vs), 1621 (m), 1570 (w), 1507 (w), 1460 (m), 1391 (s), 1345 (w), 1309 (w), 1256 (w), 1201 (w), 1056 (w), 1048 (w), 1017 (w), 1002 (w), 962 (w), 867 (w), 823 (w), 764 (m), 746 (m), 686 (w), 658 (w), 581 (w), 551 (w), 514 (w), 462 (w).

For **4@PMMA** (400 : 1): yield: 88%. FT-IR (KBr, cm^{-1}): 3627 (w), 3380 (m), 3220 (w), 3305 (w), 3070 (w), 2997 (m), 2949 (m), 2842 (w), 1732 (vs), 1625 (m), 1571 (w), 1505 (w), 1460 (w), 1392 (s), 1347 (w), 1309 (w), 1254 (w), 1201 (w), 1057 (w), 1046 (w), 1018 (w), 1002 (w), 961 (w), 867 (w), 822 (w), 767 (m), 743 (m), 684 (w), 652 (w), 585 (w), 554 (w), 512 (w), 465 (w).

Synthesis of PNBE-supported metallopolymer-type hybrid materials Poly(NBE-1), Poly(NBE-2), Poly(NBE-3) and Poly(NBE-4)

The homogeneous copolymerization of NBE and each of the complexes **1–4** with a stipulated feeding molar ratio (200 : 1, 400 : 1, 600 : 1 or 800 : 1) in activation with H–Grubbs II was carried out in a Fisher-Porter glass reactor and protected by dry N_2. To a solution of the complex {[Ln_3(L)$_4Cl_4$(MeOH)-(H_2O)]·Cl} (0.02 mmol, Ln = La (**1**), 35.4 mg; Ln = Eu (**2**), 35.8 mg; Ln = Tb (**3**), 36.2 mg or Ln = Gd (**4**), 36.4 mg) in dry $CHCl_3$ (30 mL), NBE (8 mmol, 752 mg) and H–Grubbs II (1.5 mol% of NBE; 11.3 mg, added in three times: 7 mg, 2.3 mg and 2 mg, respectively) were added, and the resulting homogeneous solution was purged with N_2 for 10 min and

sealed under a reduced N_2 atmosphere. The mixture was stirred at RT for 72 h. Subsequently, ethyl vinyl ether (1 mL) was added to quench the reaction. Each of the obtained products was precipitated as a viscous substance by slow dropping into cold EtOH. The resulting solids were collected by filtration and dried at 45 °C under vacuum to a constant weight, respectively.

For **Poly(NBE-1)** (400 : 1): yield: 79%. FT-IR (KBr, cm^{-1}): 3313 (b), 2943 (m), 2862 (s), 2733 (w), 2603 (m), 2530 (w), 2495 (w), 1994 (w), 1772 (m), 1710 (m), 1662 (w), 1616 (w), 1490 (s), 1448 (s), 1348 (w), 1257 (s), 1205 (m), 1145 (w), 1037 (s), 966 (vs), 912 (w), 864 (w), 821 (s), 744 (w), 698 (vs), 671 (w), 580 (w), 497 (w), 439 (w). ^{1}H NMR (400 MHz, DMSO-δ_6–$CDCl_3$, v/v = 10 : 1): δ (ppm) 13.17 (s, 4H, –NH), 8.28 (m, 1H, –OH), 7.60 (b, 8H, –Ph), 7.53 (b, 2H, –Ph), 7.46 (b, 2H, –Ph), 7.25 (b, 8H, –Ph), 7.06 (b, 1H, –Ph), 6.86 (b, 2H, –Ph), 6.78 (b, 1H, –Ph), 5.72 (m, 4H, –Ph), 5.54 (b, 4H, –CH═C), 5.27 (s, 150H, –CH═CH– (Z)), 5.14 (s, 150H, –CH═CH– (E)), 4.90 (d, 4H, –CH═CH_2), 4.79 (d, 4H, –CH═CH_2), 3.94 (m, 3H, MeOH), 3.93 (m, 12H, –OMe), 3.36 (m, 8H, –CH_2–C═C), 2.72 (s, 150H, –CH), 2.37 (s, 150H, –CH), 1.73 (m, 450H, –CH_2), 1.28 (s, 300H, –CH_2), 0.95 (m, 150H, –CH_2).

For **Poly(NBE-2)** (400 : 1): yield: 74%. FT-IR (KBr, cm^{-1}): 3310 (b), 2941 (m), 2862 (s), 2735 (w), 2600 (m), 2534 (w), 2492 (w), 1990 (w), 1773 (m), 1713 (m), 1660 (w), 1614 (w), 1495 (s), 1447 (s), 1345 (m), 1255 (s), 1204 (m), 1149 (w), 1036 (s), 967 (vs), 910 (w), 865 (w), 818 (w), 747 (w), 674 (w), 580 (w), 493 (w), 431 (w).

For **Poly(NBE-3)** (200 : 1, 400 : 1, 600 : 1 or 800 : 1): yield: 55% (200 : 1); 77% (400 : 1); 82% (600 : 1); 85% (800 : 1). FT-IR (KBr, cm^{-1}): 3313 (b), 2945 (m), 2862 (s), 2734 (w), 2603 (m), 2530 (w), 2496 (w), 1994 (w), 1773 (m), 1710 (m), 1660 (w), 1616 (w), 1491 (s), 1448 (s), 1347 (m), 1257 (s), 1206 (m), 1145 (w), 1036 (s), 968 (vs), 912 (w), 864 (w), 820 (w), 743 (w), 670 (w), 580 (w), 497 (w), 438 (w).

For **Poly(NBE-4)** (400 : 1): yield: 73%. FT-IR (KBr, cm^{-1}): 3311 (b), 2943 (m), 2860 (s), 2733 (w), 2601 (m), 2530 (w), 2490 (w), 1994 (w), 1772 (m), 1711 (m), 1662 (w), 1616 (w), 1491 (s), 1448 (s), 1347 (m), 1257 (s), 1205 (m), 1148 (w), 1037 (s), 965 (vs), 912 (w), 864 (w), 820 (w), 745 (w), 671 (w), 582 (w), 497 (w), 438 (w).

3. Results and discussion

Synthesis and characterization of the ligand HL and its series of complex monomers {$[Ln_3(L)_4Cl_4(MeOH)(H_2O)]\cdot Cl$} (Ln = La, 1; Ln = Eu, 2; Ln = Tb, 3 or Ln = Gd, 4)

As shown in Scheme 1, 5-allyl-2-hydroxy-3-methoxy-benzaldehyde was synthesized by the Williamson synthesis and the subsequent *para* Claisen rearrangement with *o*-vanillin and allyl bromide as the starting materials in the presence of anhydrous K_2CO_3 as in the literature.[17] The diallyl-modified Salen-type Schiff-base precursor $\mathbf{H_2L^0}$ was obtained from the condensation reaction of *o*-phenylenediamine with 5-allyl-2-hydroxy-3-methoxy-benzaldehyde in a 1 : 2 molar ratio, while in refluxing absolute MeOH, the precursor $\mathbf{H_2L^0}$ was successfully converted into the off-white benzimidazole-type ligand **HL** in a good yield of 70%. Furthermore, reaction of the allyl-modified benzimidazole-type ligand **HL** and $LnCl_3\cdot 6H_2O$ (Ln = La, Eu, Tb or Gd) in different metal to ligand molar ratios (1 : 1, 4 : 3 1 : 2 or 1 : 4) afforded similar series of homo-leptic trinuclear complexes {$[Ln_3(L)_4Cl_4(MeOH)(H_2O)]\cdot Cl$} (Ln = La, **1**; Ln = Eu, **2**; Ln = Tb, **3** or Ln = Gd, **4**), respectively, despite the slight difference in yields. Similar to the good solubility of the allyl-modified benzimidazole-type ligand **HL** in common organic solvents except for water, complexes **1–4** are also soluble in slightly-polar organic solvents due to the introduction of flexible allyl groups together with the charge of the two components (the cationic $[Ln_3(L)_4Cl_4(MeOH)(H_2O)]^+$ part and one free Cl^- anion) in each of the four complexes.

The Schiff-base precursor $\mathbf{H_2L^0}$, the benzimidazole-type ligand **HL**, and its series of complexes **1–4** were well characterized by EA, FT-IR, ^{1}H NMR and ESI-MS. In the FT-IR spectra,

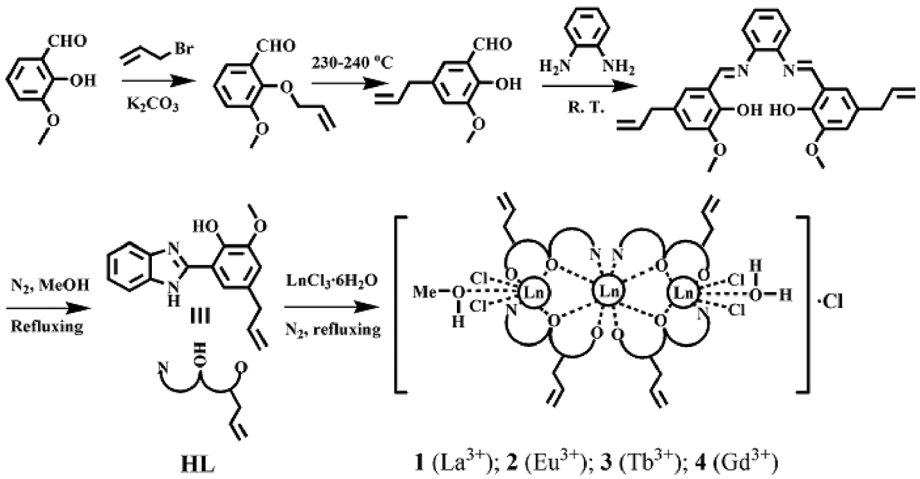

Scheme 1 Reaction scheme for the synthesis of the diallyl-modified Salen-type Schiff-base precursor H_2L^0, the allyl-modified benzimidazole-type ligand HL and its series of homo-leptic Ln_3-arrayed complexes 1–4.

two characteristic strong absorptions at 1620–1624 and 993–1000 cm^{-1} attributed to the ν vibration and the ω vibration of the terminal active $=CH_2$ groups from allyl substituents were observed for the precursor $\mathbf{H_2L^0}$, the ligand **HL** and complexes **1–4**, respectively. As to the ^1H NMR spectrum identification of the precursor $\mathbf{H_2L^0}$ or the ligand **HL**, a similar intra-molecular resonance-assisted hydrogen bonded (RAHB) O–H···N proton resonance (δ = 13.16 ppm for $\mathbf{H_2L^0}$ or δ = 11.09 ppm for **HL**) and the well-kept proton resonances (δ = 6.01, 5.10 and 3.36 ppm for $\mathbf{H_2L^0}$ or δ = 6.09, 5.17 and 3.44 ppm for **HL**) of the functional allyl groups were exhibited. Nevertheless, the replacement of the typical –CH=N– proton resonance (δ = 8.71 ppm) for the precursor $\mathbf{H_2L^0}$ with the typical –NH proton resonance (δ = 12.99 ppm) for the ligand **HL** endowed their distinctive differences. The ^1H NMR spectrum (shown in Fig. 1) of the *anti*-ferromagnetic trinuclear La_3-arrayed complex **1**, due to the coordination of La^{3+} ions, showed a slightly spread shift (δ from 13.17 to 3.33 ppm) of the proton resonances of the ligands relative to that of the free ligand **HL** (δ from 12.99 to 3.44 ppm). Moreover, besides the persistence of proton resonances (δ = 6.03, 5.13 and 3.33 ppm) for the terminal allyl groups of complex **1**, the presence of new proton resonances (δ = 8.24 and 3.87 ppm) from one coordinated MeOH molecule, together with the slight shift of the proton resonances of four coordinated ligands, also confirmed the formation of La_3-arrayed complex **1**. The ESI-MS spectra of the series of complexes **1–4** displayed similar patterns and exhibited the strong mass peak at *m*/*z* 1725.86 (**1**), 1765.02 (**2**), 1785.92 (**3**) or 1780.89 (**4**) assigned to the major species of $[Ln_3(L)_4Cl_4(MeOH)(H_2O)]^+$ of complexes **1–4**, respectively. These observations further indicate that each of the discrete homo-leptic Ln_3-arrayed units is retained in the corresponding dilute MeCN solution.

The solid state structure of **3**·2MeOH·4H_2O as the representative of complexes **1–4** was determined by single-crystal X-ray diffraction analysis, and its crystallographic data and selected bond parameters are presented in Tables 1 and 1S,† respectively. Complex **3**·2MeOH·4H_2O crystallizes in the triclinic space group $P\bar{1}$. For **3**·2MeOH·4H_2O, the smallest symmetric unit is composed of one cation $[Tb_3(L)_4Cl_4(MeOH)(H_2O)]^+$, one free Cl^- anion, two solvates MeOH and four solvates H_2O. As shown in Fig. 2, four deprotonated $(\mathbf{L})^-$ ligands chelate to three Tb^{3+} ions with a non-linear linkage (Tb1–Tb2–Tb3 angle of 144.51(5)°), where the central Tb^{3+} ion (Tb2) is bridged by two phenolic O atoms (O1 and O5 or O3 and O7) from the corresponding two deprotonated $(\mathbf{L})^-$ ligands to the two terminal Tb^{3+} ions (Tb1 or Tb3), respectively. The three Tb^{3+} ions exhibit three kinds of different coordination environments, where the unique central Tb^{3+} ion (Tb2) is eight-coordinate and bound by two sets of the phenolic O atom (O5 or O7) and the methoxy O atom (O6 or O8) from two different deprotonated $(\mathbf{L})^-$ ligands and two sets of the imidazole N (N2 or N4) and the phenolic O atom (O1 or O3) from the other two different deprotonated $(\mathbf{L})^-$ ligands. However, both of the two terminal Tb^{3+} ions (Tb1 and Tb3) with slightly different coordination environments are seven-coordinate: in addition to the imidazole N (N6 or N8) and the phenolic O atom (O5 or O7) from one deprotonated $(\mathbf{L})^-$ ligand and the phenolic O atom (O1 or O3) and the methoxy O atom (O2 or O4) from another deprotonated $(\mathbf{L})^-$ ligand, it saturates its coordination sphere from two coordinated Cl^- anions (Cl1 and Cl2 or Cl3 and Cl4) and one O10 atom from the coordinated H_2O or one O9 atom from the coordinated MeOH molecule, respectively. Two unique Tb···Tb distances of 3.8563(35) and 3.8368(37) Å are between the central Tb^{3+} ion (Tb2) and the two terminal Tb^{3+} ions (Tb1 and Tb3), respectively. In addition to the weak N1–H1···Cl5 H-bonding (3.045(2) Å, shown in Fig. 1S†) between the free Cl^- anion (Cl5) for charge balance with one deprotonated $(\mathbf{L})^-$ ligand, free solvates MeOH and H_2O are not bound

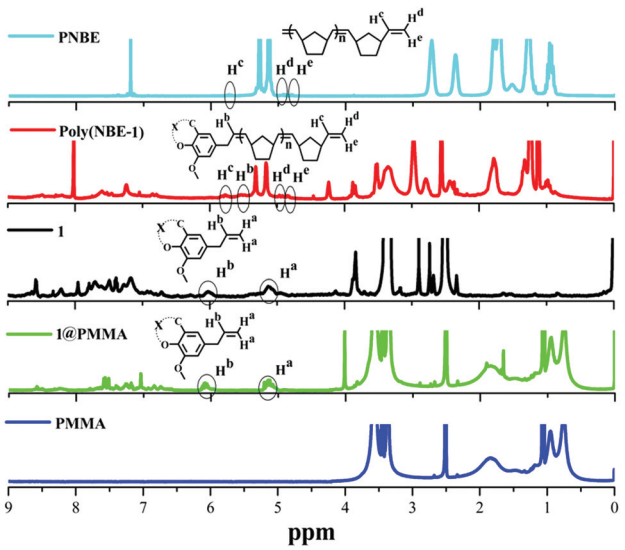

Fig. 1 ^1H NMR spectra for **PMMA**, **PNBE**, **1**, **1@PMMA** and **Poly(NBE-1)** from the feeding molar ratio of 400 : 1 in DMSO-δ_6 and/or $CDCl_3$ at RT.

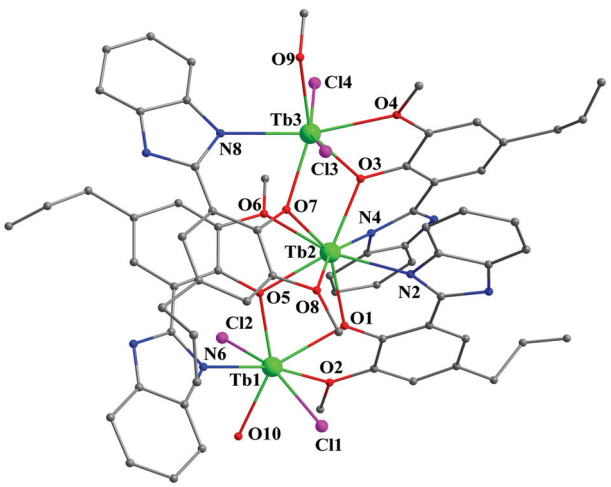

Fig. 2 Perspective drawing of the cationic part in complex **3**·2MeOH·4H_2O; H atoms, free anion Cl^- and solvates are omitted for clarity.

Table 2 The photophysical properties of the ligand **HL** and its complexes **2–4** at 1 × 10^{-5} M in absolute MeCN solution, the PMMA-supported doping hybrid materials **2@PMMA**, **3@PMMA** and **4@PMMA**, the PNBE-supported metallopolymer-type hybrid materials **Poly(NBE-2)**, **Poly(NBE-3)** and **Poly(NBE-4)** from the same feeding molar ratio of 400 : 1 in the solid state at RT or 77 K

Compound	Absorption λ_{ab}/nm [log(ε/dm^3 mol^{-1} cm^{-1})]	Excitation λ_{ex}/nm	Emission λ_{em}/nm	τ	Φ
HL	228 (0.57), 300 (0.53), 324 (0.36)	326	405(s)	1.67 ns	—[a]
2 (Ln^{3+} = Eu^{3+})	226 (1.55), 298 (0.97), 330 (0.59)	272, 317, 359	428(w)	<1 ns	$<10^{-5}$
3 (Ln^{3+} = Tb^{3+})	226 (1.61), 296 (0.95), 332 (0.58)	273, 346	488, 543, 583, 622	104.54 μs	0.72
4 (Ln^{3+} = Gd^{3+})	224 (1.75), 300 (1.00), 330 (0.61)	274, 317, 359	426(m)	1.51 ns	—[a]
		272, 318, 359	433(s)	29.4 μs (77 K)	—[a]
2@PMMA	212, 304, 347	282(sh), 346	430(w)	—[a]	—[a]
3@PMMA	214, 298, 350	303, 370	492, 548, 588, 623	291.50 μs	0.76
4@PMMA	212, 304, 348	281(sh), 343	426(m)	1.38 ns	—[a]
		304, 361	450(s)	89.0 μs (77 K)	—[a]
Poly(NBE-2)	208, 222, 304, 341	320, 383	443(w)	—[a]	—[a]
Poly(NBE-3)	210, 223, 304, 342	325, 395	491, 547, 586, 624	451.04 μs	0.83
Poly(NBE-4)	209, 224, 303, 344	318, 381	440(m)	0.92 ns	—[a]
		317, 383	455(s)	174.8 μs (77 K)	—[a]

[a] The lifetime or the quantum yield of the emission is too weak or unnecessary to be determined.

to the homo-leptic framework, and they exhibit no observed interactions with the host structure. It is worth noting that the homo-leptic trinuclear host structure in **3**·2MeOH·4H_2O is distinctively different from the reported structures of mononuclear Ln-arrayed or homo-leptic binuclear Ln_2-arrayed complexes[23] while it is comparable to Cl^--dependent homo-leptic Ln_3-arrayed structures[24] based on the analogue Br-modified benzimidazole-type ligand. This result shows that the discrete homo-leptic Ln_3-arrayed host structure of complex **3**·2MeOH·4H_2O is stable and not strictly relying on the stoichiometries as in the literature,[23] especially with the involvement of electron-donating allyl and not the electron-withdrawing Br group. Moreover, all the four functional allyl groups with C=C bond lengths of 1.297(10)–1.304(19) Å for the typical C=C bonds in complex **3**·2MeOH·4H_2O are well retained.

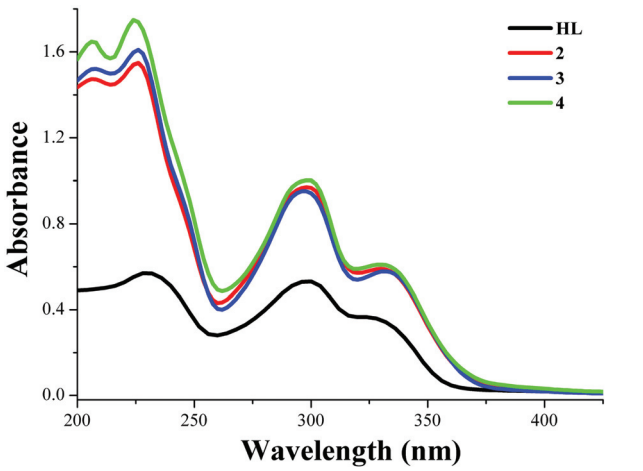

Fig. 3 UV-visible absorption spectra of the allyl-modified benzimidazole-type ligand **HL** and its Ln_3-arrayed complexes **2–4** in MeCN solution at 1 × 10^{-5} M at RT.

Photophysical properties and energy transfer of the series of complexes {[Ln_3(L)$_4$$Cl_4$(MeOH)($H_2O$)]·Cl} (Ln = Eu, 2; Ln = Tb, 3 or Ln = Gd, 4) in solution

The photophysical properties of the ligand **HL** and its complexes **2–4** have been examined in dilute MeCN solution at RT or 77 K, and summarized in Table 2 and Fig. 3 and 4. As shown in Fig. 3, similar ligand-centered solution absorptions (224–226, 296–300 and 330–332 nm) of complexes **2–4** in the UV-visible region are observed, where all the intra-ligand low-energy π–π* transition absorptions are red-shifted upon coordination of Ln^{3+} ions compared to that (324 nm) of the free ligand **HL**. For complex **2**, photoexcitation (λ_{ex} = 359 nm) of the chromophore just gives rise to weak residual visible emission (λ_{em} = 428 nm) assigned to the π–π* ligand transition, and no characteristic Eu^{3+}-based line-like emissions are observed. In contrast, for complex **3**, as shown in Fig. 4, the ligand-centered emission is not detectable in the emission spectrum, while strong characteristic ligand-field splitting emissions of Tb^{3+} ions from the emitting level ($^5D_4$) to the ground multiple ^7F_J (J = 6, 5, 4, 3) are exhibited, respectively. The strongest

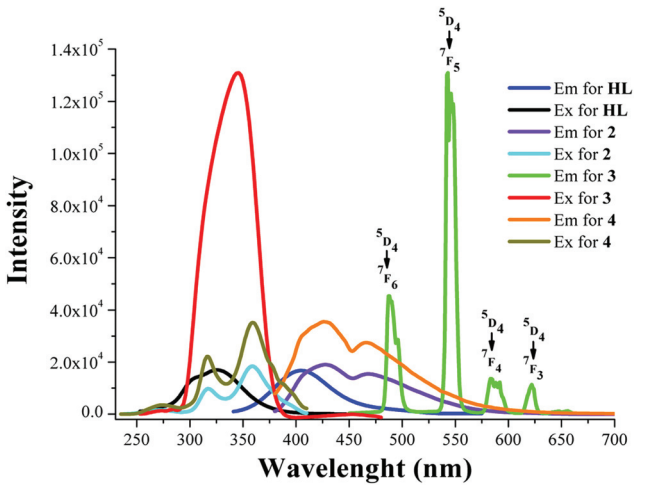

Fig. 4 Visible emission and excitation spectra of the ligand **HL** and its complexes **2–4** in MeCN solution at 1 × 10^{-5} M at RT.

emission (λ_{em} = 543 nm) based on the hyper-sensitive $^5D_4 \rightarrow {}^7F_5$ transition, together with the second maximum peak at 488 nm corresponding to the $^5D_4 \rightarrow {}^7F_6$ transition, endows the bright green solution luminescence with a CIE (Commission International De L'Eclairage) chromatic coordinate x = 0.304 and y = 0.599 for complex **3**.

It is of special interest to explore the detailed mechanism of the energy transfer process for the two complexes **2** and **3**. As a suitable reference compound, the Gd_3-arrayed complex **4** allows further study of the chromophore luminescence in the absence of energy transfer, because the Gd^{3+} ion has no energy levels below 32 150 cm^{-1} and therefore cannot accept any energy from the excited state of the chromophore.[25] Different from the typical fluorescence (λ_{em} = 426 and τ = 1.51 ns) at RT, as shown in Fig. 2S,† complex **4** exhibits phosphorescence (λ_{em} = 433 and τ = 29.4 μs) at 77 K, from which the triplet ($^3\pi$–π^*) energy level at 23 095 cm^{-1} is obtained. With regard to the singlet ($^1\pi$–π^*) energy level (28 736 cm^{-1}) estimated by the lower wavelength of its UV-visible absorbance edge, so the larger energy gap ΔE_1 (5641 cm^{-1}, $^1\pi$–π^*–$^3\pi$–π^*) than 5000 cm^{-1}, as shown in Fig. 5, endows the effective inter-system crossing process according to Reinhouldt's empirical rule.[26] Further by checking the energy level match between the ligand-based $^3\pi$–π^* energy level (23 095 cm^{-1}) and the first excited state level of Eu^{3+} or Tb^{3+} ions, in spite of the energy gap (ΔE_2 = 5809 nm) for complex **2**, it is actually large enough to go beyond the reasonable range of 2500–4000 cm^{-1} from Latva's empirical rule.[27] The possible heavy non-radiative de-activation results in complete quenching of the characteristic Eu^{3+}-based emissions. As to complex **3**, the relatively smaller energy gap (ΔE_2 = 2550 nm) within the ideal 2500–4500 cm^{-1} range[27] confirms the suitability of the allyl-modified benzimidazole-type ligand **HL** as a sensitizer for Tb^{3+} ions. The Tb^{3+} ion ($^5D_4$) lifetime of complex **3** (Fig. 6) under excitation of 346 nm has been measured to be τ_{obs} = 104.54 μs, which is not one among the longest so far reported Tb^{3+}-complexes,[28] while an attractive high quantum yield ($\Phi_{overall}$, 72%) for complex **3** in solution is obtained. This should be mainly attributed to the suitable energy level match and the additive electronic communication between three Tb^{3+} centers in complex **3** despite the vibrational quenching[7] from OH-containing oscillators (MeOH and H_2O) in the inner coordination spheres of the two terminal Tb^{3+} ions.

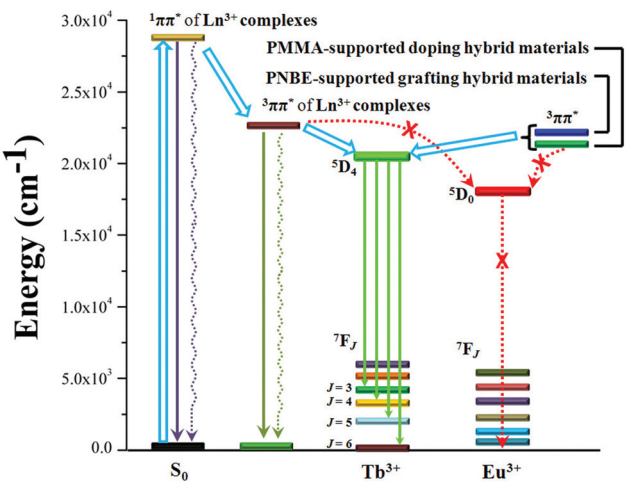

Fig. 5 Schematic energy level diagram and energy transfer process of Eu^{3+} or Tb^{3+} for complexes **2–3** in solution and the PMMA-supported doping or PNBE-supported metallopolymer-type hybrid materials based on complexes **2–3** with the same feeding molar ratio of 400 : 1 in the solid state.

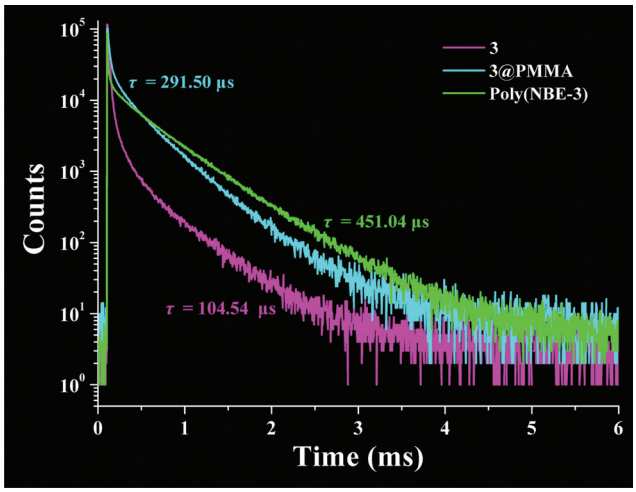

Fig. 6 Luminescence decay profiles for complex **3** in solution and the hybrid materials **3@PMMA** and **Poly(NBE-3)** from the same feeding molar ratio of 400 : 1 in the solid state with emission monitored at approximately 545 nm.

Synthesis and characterization of PMMA-supported doping hybrid materials 1@PMMA, 2@PMMA, 3@PMMA and 4@PMMA and PNBE-supported metallopolymer-type hybrid materials Poly(NBE-1), Poly(NBE-2), Poly(NBE-3) and Poly(NBE-4)

In consideration of the excellent performance of PMMA as one of the popular polymer matrices with low cost, low optical absorbance and good mechanical properties,[29] it is of interest to explore the radical polymerization behaviors of the series of Ln_3-arrayed complexes **1–4** containing four active allyl groups as the complex monomers like those[16] containing active vinyl groups with MMA in activation with AIBN. To our dismay, the copolymerization does not effectively occur as expected, where each of the complexes **1–4** is just physically doped into the *in situ* formed PMMA matrix from homo-polymerization of MMA, exclusively giving the series of PMMA-supported doping hybrid materials **1@PMMA**, **2@PMMA**, **3@PMMA** and **4@PMMA**, as shown in Scheme 2, respectively. As to the isolated hybrid materials, in the FT-IR spectra from the simple combination of characteristic absorptions from each of **1–4** and PMMA, the intense absorption band at 1731–1732 cm^{-1} attributed to the ν(C=O) vibration of PMMA appears, and the characteristic absorptions at 1621–1625 and 1000–1002 cm^{-1} assigned to the ν(allyl) vibration and the ω(allyl) vibration of complexes **1–4** are weakened but well kept due to the low concentration doping. Nevertheless, the absence of the band

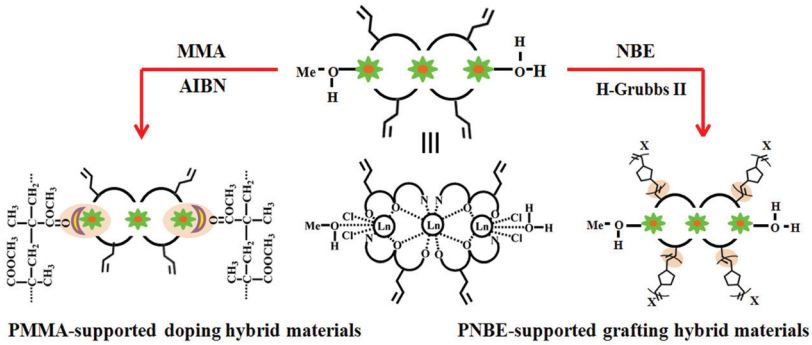

Scheme 2 Reaction scheme for the synthesis of PMMA-supported doping hybrid materials **1@PMMA**, **2@PMMA**, **3@PMMA** and **4@PMMA** and PNBE-supported metallopolymer-type hybrid materials **Poly(NBE-1)**, **Poly(NBE-2)**, **Poly(NBE-3)** and **Poly(NBE-4)**.

absorptions in the range of 3373–3390 cm^{-1} attributed to the coordinated MeOH and H_2O in complexes **1–4**, together with the slight blue-shift by 3–4 cm^{-1} of ν(C═O) vibrations (1731–1732 cm^{-1}) of **1@PMMA**, **2@PMMA**, **3@PMMA** and **4@PMMA** than that (1728 cm^{-1}) of pure PMMA indicates that the two coordinated MeOH and H_2O should be replaced by carbonyl groups from PMMA through physical doping (also shown in Scheme 2). Especially based on the ^{1}H NMR spectrum (also shown in Fig. 1) of *anti*-ferromagnetic **1@PMMA**, the well combined and almost not shifted proton resonances of the coordinated benzimidazole-type ligand $(\mathbf{L})^-$ and PMMA are unambiguously identical to those of complex **1** and PMMA, respectively. The results indicate that the series of complexes **1–4** with active allyl groups cannot be copolymerized with MMA in the presence of AIBN through the free-radical mechanism,[16] probably due to the degradative chain transfer[30] of the flexible allyl groups, from which lower reactivity of the resonance-stabilized monomeric radical formed from those complex monomers than that of MMA leads to much less tendency to initiate a new polymer chain. It is worthy of special note that the quantitative ^{1}H NMR analysis of **1@PMMA** further shows a distinctively lower molar ratio of 110 : 1 than the initial feed molar ratio (400 : 1) of MMA with **1**, which should be due to the loss of MMA from oligomeric PMMA.

Assisted by the success of homo-polymerization of NBE or it derivatives[31] and their copolymerization[17,32] with many other C═C-containing (including allyl groups) functional monomers using the typical ROMP in activation with Grubbs-type catalysts, copolymerization of the series of Ln_3-arrayed complexes **1–4** containing four active allyl groups with NBE was carried out in absolute $CHCl_3$ at RT in activation with H–Grubbs II (also in Scheme 2). Undoubtedly, all the copolymerizations were complete after 72 h as expected, from which each of the benzimidazole-based Ln_3-arrayed units with four functional allyl groups is covalently bonded to the PNBE polymeric backbone; thus the first example of metallopolymers based on the homo-trinuclear Ln_3-arrayed units has been constructed to date. The isolated metallopolymer-type hybrid materials **Poly(NBE-1)**, **Poly(NBE-2)**, **Poly(NBE-3)** and **Poly(NBE-4)** with a Wolf Type II fashion[33] are also well characterized by FT-IR, ^{1}H NMR and GPC. In the FT-IR spectra, the characteristic absorptions of unsaturated C═C bonds from allyl groups of complexes **1–4** completely disappear. The ^{1}H NMR spectrum analysis of the *anti*-ferromagnetic **Poly(NBE-1)** (also shown in Fig. 1) shows the combined proton resonances (δ = 13.17–0.95 ppm) of the coordinated benzimidazole-type ligand $(\mathbf{L})^-$ and NBE, where the proton resonances of new –CH═CH– within at 5.54 ppm and the terminal –C═CH_2 at 4.90 and 4.79 ppm from NBE-ring-opening groups of **1**, together with those of the *Z*-mode –CH═CH– at 5.27 ppm and the *E*-mode –CH═CH– at 5.14 ppm from PNBE, are displayed, respectively. As shown in Table 2S,† the number-average molecular weights (M_n) and polydispersity indexes (PDI = M_w/M_n) of the series of PNBE-supported grafting hybrid materials from different feeding molar ratios are in the range of 20 020–25 592 g mol^{-1} and 2.11–2.58, respectively, where those relatively lower molecular weights in the 10^4 g mol^{-1} magnitude could endow good solubility and facilitated film-forming. Especially for the obtained hybrid materials **Poly(NBE-3)** from different feeding molar ratios (200 : 1, 400 : 1, 600 : 1 and 800 : 1) with NBE to **3**, there is an almost linear relationship between the molecular weights and the feeding molar ratios, suggesting a random bonding and homogeneous distribution of **3** along the polymeric backbone.[34]

PXRD patterns of the two series of $\{[Ln_3(L)_4Cl_4(MeOH)(H_2O)]\cdot Cl\}$-containing doping and grafting hybrid materials (as shown in Fig. 7a and 7b) show only amorphous peaks of PMMA and PNBE, respectively. This suggests that in the two kinds of hybrid materials with good film-forming property, the Ln_3-arrayed benzimidazole-type complex unit is homogeneously distributed into the PMMA matrix with complicated weak interactions or the PNBE matrix with strong covalent bonds between, respectively, especially under the conditions of low concentrations. Moreover, a TG analysis of the series of PMMA-supported doping hybrid materials shows an increase of about 25 °C for the T_{onset} in comparison with the pure PMMA, as shown in Fig. 8, and a relatively slight increase (15 °C) is observed for another series of PNBE-supported metallopolymer-type hybrid materials as compared with pure PNBE. However, decomposition with maxima around a much

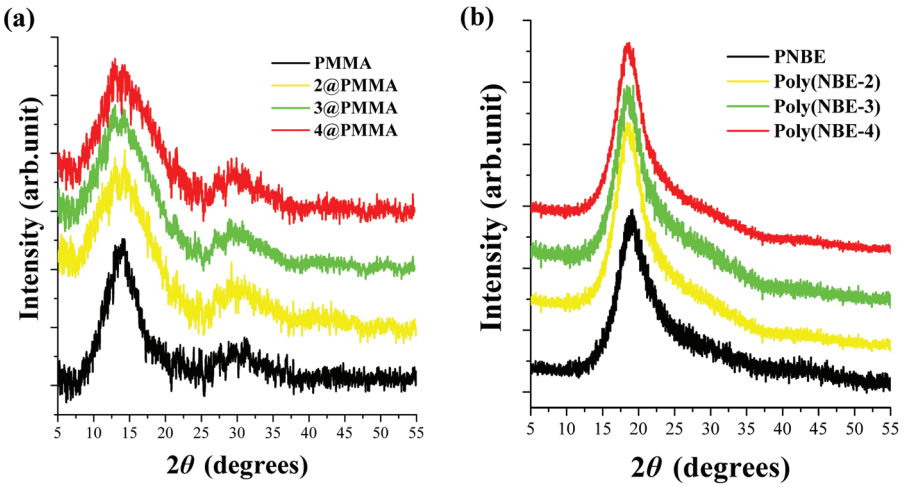

Fig. 7 PXRD patterns of PMMA and its series of PMMA-supported doping hybrid materials **2@PMMA**, **3@PMMA** and **4@PMMA** (a), PNBE and its series of PNBE-supported metallopolymer-type hybrid materials **Poly(NBE-2)**, **Poly(NBE-3)** and **Poly(NBE-4)** (b) from the same feeding molar ratio of 400 : 1 in the solid state.

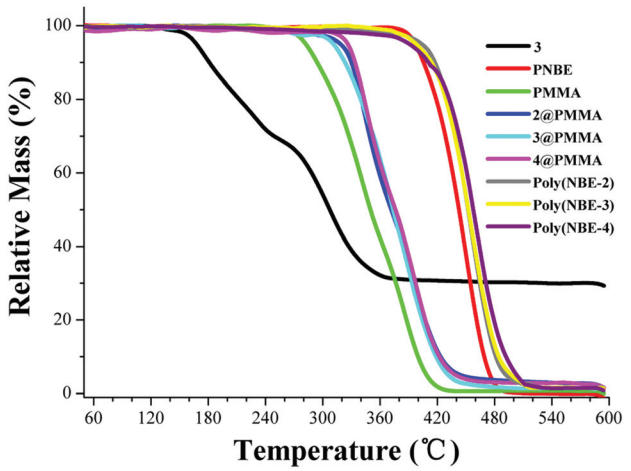

Fig. 8 TG curves of complex **3**, PMMA, PNBE, and the two series of PMMA-supported doping hybrid materials **2@PMMA**, **3@PMMA** and **4@PMMA** and PNBE-supported metallopolymer-type hybrid materials **Poly(NBE-2)**, **Poly(NBE-3)** and **Poly(NBE-4)** from the same feeding molar ratio of 400 : 1 in the solid state.

higher temperature interval (452–458 °C) for the PNBE-supported metallopolymer-type hybrid materials than that (366–372 °C) for the PMMA-supported doping hybrid materials is exhibited, and both are distinctively higher than that (278 °C) of the representative complex **3**. These observations further demonstrate that the thermal stabilities of the two kinds of hybrid materials are essentially improved by doping or grafting, and the metallopolymer-type hybrid materials are more stable relative to those physical doping hybrid materials.

Photophysical properties of the two series of hybrid materials 2@PMMA, 3@PMMA and 4@PMMA and Poly(NBE-2), Poly(NBE-3) and Poly(NBE-4) in the solid state

For the two series of hybrid materials, their photophysical properties in the solid state at RT or 77 K have been examined, and are also summarized in Table 2 and Fig. 9–12 and 2S.† As shown in Fig. 9, DR spectra of both the PMMA-supported doping and PNBE-supported metallopolymer-type hybrid materials from complexes **2–4** exhibit relatively broader absorption bands than those of complexes **2–4** in solution, where the absorptions at 212–214, 298–304 and 347–350 nm or 208–210, 222–224, 303–304 and 341–344 nm in the UV-visible region should be assigned to electronic transitions from the organic moieties of both the coordinated benzimidazole-type ligands and PMMA or PNBE, respectively. Due to the characteristic absorption bands of Eu^{3+}, Tb^{3+} or Gd^{3+} ions commonly appearing above 1000 nm,[35] they are not discerned in the corresponding samples. Upon excitation of the chromophore's absorption band (λ_{ex} = 346 nm for **2@PMMA** or λ_{ex} = 343 nm

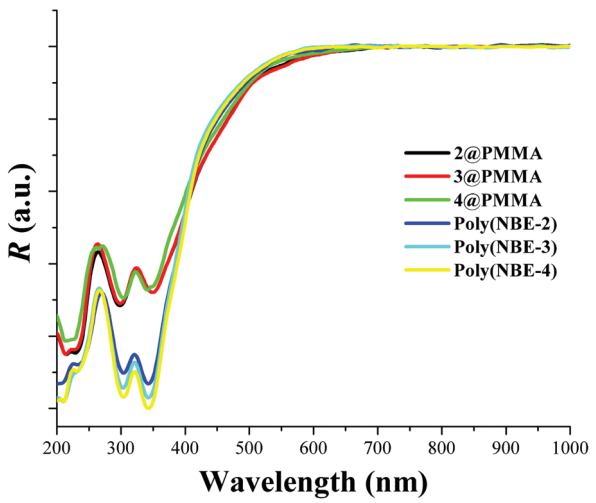

Fig. 9 DR spectra of the two series of PMMA-supported doping hybrid materials **2@PMMA**, **3@PMMA** and **4@PMMA** and PNBE-supported metallopolymer-type hybrid materials **Poly(NBE-2)**, **Poly(NBE-3)** and **Poly(NBE-4)** from the same feeding molar ratio of 400 : 1 in the solid state.

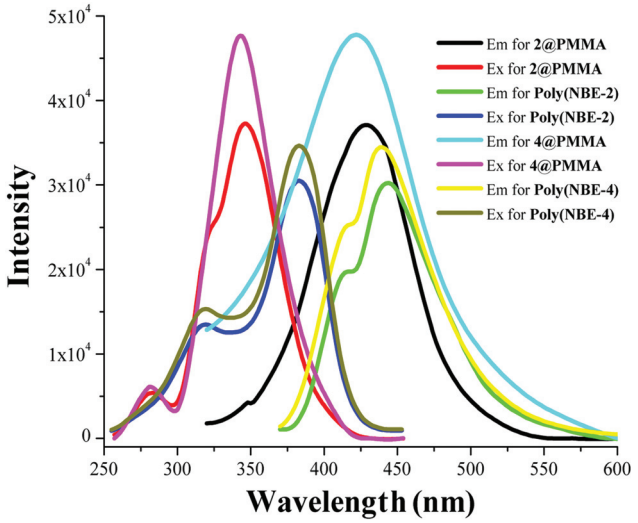

Fig. 10 Visible emission and excitation spectra of **2@PMMA** and **4@PMMA**, or **Poly(NBE-2)** and **Poly(NBE-4)** with the feeding molar ratio of 400 : 1 in the solid state at RT.

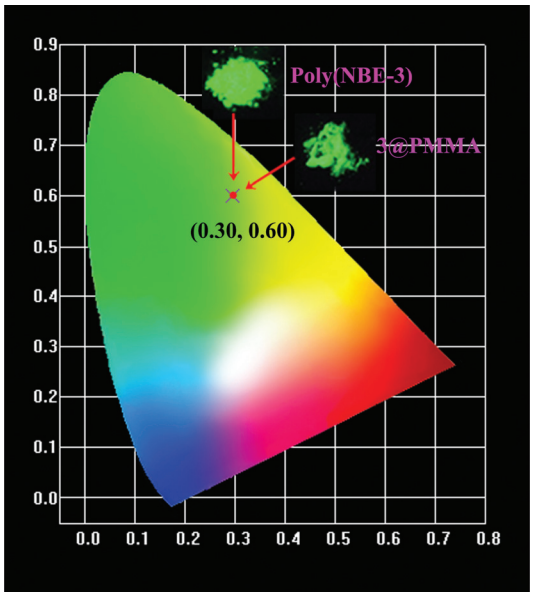

Fig. 12 CIE chromaticity graphs with the same color coordinate (x = 0.30, y = 0.60) for the emissions of **3@PMMA** and **Poly(NBE-3)** with the feeding molar ratio of 400 : 1 in the solid state.

for **4@PMMA**), both **2@PMMA** and **4@PMMA** in the solid state also exhibit the ligand-based emissions shown in Fig. 10, and **3@PMMA** also gives rise to the strong characteristic ligand-field splitting while also high color-purity green emissions ($^5D_4 \rightarrow {}^7F_J$, J = 6, 5, 4, 3 shown in Fig. 11a and a CIE coordinate of x = 0.302 and y = 0.598 shown in Fig. 12) of Tb^{3+} ions. Especially for the solid **3@PMMA**, the lifetime value (τ = 291.50 μs also shown in Fig. 6) is found to distinctively increase relative to that of complex **3** in solution, which should be assigned to the newly coupling interactions between –C═O of PMMA and the OH-containing oscillators around Tb^{3+} ions to suppress the multiphonon relaxation.[36] Similarly, for the PNBE-supported metallopolymer-type hybrid material **Poly(NBE-3)**, the ligand-centered emission is also completely quenched, and stronger high color-purity green emission with a CIE coordinate of x = 0.301 and y = 0.600 (also shown in Fig. 12) of Tb^{3+} ions is observed, as shown in Fig. 11b.

It is worth noting that the maximum excitation positions (λ_{ex} = 383 nm for **Poly(NBE-2)**, λ_{ex} = 395 nm for **Poly(NBE-3)** or λ_{ex} = 381 nm for **Poly(NBE-4)**) for the PNBE-supported grafting hybrid materials in the solid state are all distinctively red-shifted as compared to the solution spectra of complex monomers **2–4** or the solid spectra of the PMMA-supported doping hybrid materials. This result, together with the slight red-shift of the ligand-centered emission for **Poly(NBE-2)** or **Poly(NBE-4)**, suggests the increased conjugation from the formation of covalently-bonded metallopolymers.[37] Moreover, the extension of the PNBE-based backbone for **Poly(NBE-3)** changes the ligand electric fields around the Tb^{3+} ions, leading to the further increase of lifetime value (τ = 451.04 μs also shown in Fig. 6). From the viewpoint of energy transfer, the weak coupling interactions in **3@PMMA** or the strong covalent bonding in **Poly(NBE-3)** could probably recombine the charge carrier at the Tb^{3+}-related trap site[38] in the corresponding polymer matrix, endowing an effective decrease of the $^3\pi$–π^* energy level (22 222 cm^{-1} or 21 978 cm^{-1}) of the chromo-

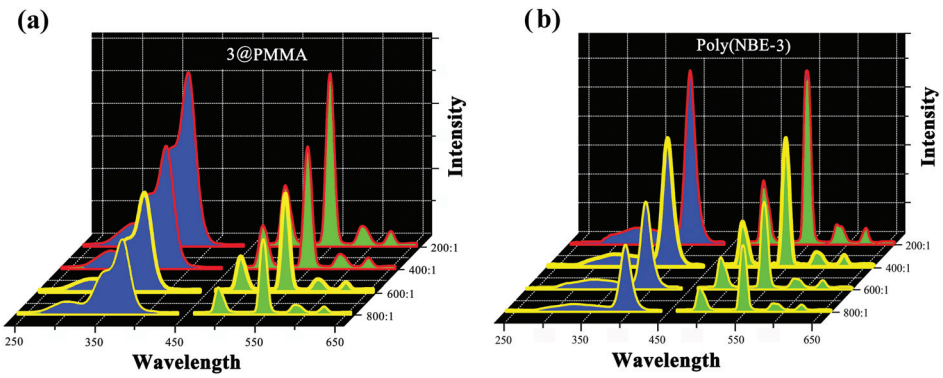

Fig. 11 Emission and excitation spectra of the hybrid materials **3@PMMA** (a) or **Poly(NBE-3)** (b) from different feeding molar ratios (200 : 1, 400 : 1, 600 : 1 and 800 : 1) in the solid state at RT.

phore to strengthen the ligand-to-metal energy transfer. These results based on a more suitable energy match (also shown in Fig. 5) are well in accordance with the relatively larger quantum yields ($\Phi_{overall}$, 76% for **3@PMMA** or 83% for **Poly(NBE-3)**). Noticeably, the emission spectra of both **3@PMMA** (λ_{ex} = 370 nm) and **Poly(NBE-3)** (λ_{ex} = 395 nm) from Tb_3-arrayed complex **3** at a variety of feeding molar ratios (200 : 1, 400 : 1, 600 : 1 and 800 : 1) exhibit the same well-defined emission peaks characteristic of the $^5D_4 \rightarrow {}^7F_J$ (J = 6, 5, 4, 3) transitions of Tb^{3+} ions, as shown in Fig. 11. Although there is an almost linear relationship between the hyper-sensitive emission intensity and the feeding molar ratio, the concentration self-quenching[39] for the series of doping hybrid materials **3@PMMA** at 400 : 1 is effectively prevented from the formation of uniform grafting hybrid materials **Poly(NBE-3)**.

4. Conclusion

Through the self-assembly from the allyl-modified benzimidazole-type ligand **HL** and $LnCl_3{\cdot}6H_2O$, a series of homo-leptic Ln_3-arrayed complexes $\{[Ln_3(L)_4Cl_4(MeOH)(H_2O)]{\cdot}Cl\}$ (Ln = La, **1**; Ln = Eu, **2**; Ln = Tb, **3** or Ln = Gd, **4**) are obtained, respectively, in which energy transfer mechanism reveals the suitable energy level match for Tb_3-arrayed complex **3** with efficient green luminescence ($\Phi_{overall}$ = 72%). Moreover, each of these complex monomers **1–4** cannot be copolymerized with MMA from the radical polymerization, while can be effectively copolymerized with NBE through ROMP, giving two kinds of PMMA-supported doping hybrid materials **1@PMMA**, **2@PMMA**, **3@PMMA** and **4@PMMA** and PNBE-supported metallopolymer-type hybrid materials **Poly(NBE-1)**, **Poly(NBE-2)**, **Poly(NBE-3)** and **Poly(NBE-4)** respectively. For both **3@PMMA** and **Poly(NBE-3)** with high color-purity characteristic emissions of Tb^{3+} ions, significantly improved physical properties, such as thermal stability, film-forming property and the luminescent property, are exhibited, and the covalent bonding endows the higher-concentration (up to 400 : 1) self-quenching. This result suggests that these hybrid materials, especially the metallopolymer-type hybrid materials, can be used as green luminescent optical fibers for practical applications of high color-purity polymer-based OLEDs.

Acknowledgements

This work was funded by the National Natural Science Foundation (21373160, 91222201, and 21173165), the Program for New Century Excellent Talents in University from the Ministry of Education of China (NCET-10-0936), the research fund for the Doctoral Program (20116101110003) of Higher Education, the Science and Technology and Innovation Project (2012KTCQ01-37) of Shaanxi Province, Graduate Innovation and Creativity Fund (Visiting Learner) of Northwest University in P. R. China.

References

1 (*a*) J. Kido and Y. Okamoto, *Chem. Rev.*, 2002, **102**, 2357; (*b*) M. A. Katkova and M. N. Bochkarev, *Dalton Trans.*, 2010, **39**, 6599.
2 (*a*) S. Sivakumar, F. C. J. M. Van Veggel and M. Raudsepp, *J. Am. Chem. Soc.*, 2005, **127**, 12464; (*b*) Q.-L. Dai, M. E. Foley, C. J. Breshike, A. Lita, S. Adrian and G. F. Strouse, *J. Am. Chem. Soc.*, 2011, **133**, 15475; (*c*) M. M. Shang, C. X. Li and J. Lin, *Chem. Soc. Rev.*, 2014, **43**, 1372.
3 (*a*) F. Wang, Y. Han, C. S. Lim, Y. H. Lu, J. Wang, J. Xu, H. Y. Chen, C. Zhang, M. H. Hong and X. G. Liu, *Nature*, 2010, **463**, 1061; (*b*) L. Armelao, S. Quici, F. Barigelletti, G. Accorsi, G. Bottaro, M. Cavazzini and E. Tondello, *Coord. Chem. Rev.*, 2010, **254**, 487; (*c*) S. Roy, A. Chakraborty and T. K. Maji, *Coord. Chem. Rev.*, 2014, **273–274**, 139; (*d*) T. W. Duan and B. Yan, *J. Mater. Chem. C*, 2014, **2**, 5098.
4 (*a*) J.-C. G. Bünzli, *Chem. Rev.*, 2010, **110**, 2729; (*b*) X. H. Wang, H. B. Chang, J. Xie, B. Z. Zhao, B. T. Liu, S. L. Xu, W. B. Pei, N. Ren, L. Huang and W. Huang, *Coord. Chem. Rev.*, 2014, **273–274**, 201; (*c*) M. C. Heffem, L. M. Matosziuk and T. J. Meade, *Chem. Rev.*, 2014, **114**, 4496.
5 E. G. Moore, A. P. S. Samuel and K. N. Raymond, *Acc. Chem. Res.*, 2009, **42**, 542.
6 P. A. Tanner and C.-K. Duan, *Coord. Chem. Rev.*, 2010, **254**, 3026.
7 J.-C. G. Bünzli and S. V. Eliseeva, in *Springer Series on Fluorescence, Vol. 7, Lanthanide Spectroscopy, Materials, and Bio-applications*, ed. P. Hänninen and H. Härmä, Springer Verlag, Berlin, Germany, 2010, vol. 7, ch. 2.
8 (*a*) B. Yan, *RSC Adv.*, 2012, **2**, 9304; (*b*) L. D. Carlos, R. A. S. Ferreira, V. De Zea Bermudez, B. Julian-Lopez and P. Escribano, *Chem. Soc. Rev.*, 2011, **40**, 536.
9 K. Binnemans, *Chem. Rev.*, 2009, **109**, 4283.
10 J. Feng and H. J. Zhang, *Chem. Soc. Rev.*, 2013, **42**, 387.
11 J. M. Stanley and B. J. Holliday, *Coord. Chem. Rev.*, 2012, **256**, 1520.
12 (*a*) J. Pei, X. L. Liu, W. L. Yu, Y. H. Lai, Y. H. Liu and R. Cao, *Macromolecules*, 2002, **35**, 7274; (*b*) A. Balamurugan, M. L. P. Reddy and M. Jayakannan, *J. Phys. Chem. B*, 2009, **113**, 14128.
13 A. Meyers, A. Kimyonok and M. Weck, *Macromolecules*, 2005, **38**, 8671.
14 (*a*) Q. Ling, Y. Song, S. J. Ding, C. Zhu, D. S. H. Chan, D.-L. Kwong, E.-T. Kang and K.-G. Neoh, *Adv. Mater.*, 2005, **17**, 455; (*b*) H. Xu, R. Zhu, P. Zhao and W. Huang, *J. Phys. Chem. C*, 2011, **115**, 15627.
15 X. Y. Chen, X. P. Yang and B. J. Holliday, *J. Am. Chem. Soc.*, 2008, **130**, 1546.
16 (*a*) J. F. Li, F. Y. Song, L. Wang, J. M. Jiao, Y. X. Cheng and C. J. Zhu, *Macromol. Rapid Commun.*, 2012, **33**, 1268; (*b*) Z. Zhang, W. X. Feng, P. Y. Su, X. Q. Lü, J. R. Song, D. D. Fan, W.-K. Wong, R. A. Jones and C. Y. Su, *Inorg. Chem.*, 2014, **53**, 5950; (*c*) Z. Zhang, W. X. Feng, P. Y. Su,

L. Liu, X. Q. Lü, J. R. Song, D. D. Fan, W.-K. Wong, R. A. Jones and C. Y. Su, *Synth. Met.*, 2015, **199**, 128; (*d*) T. Z. Miao, W. X. Feng, Z. Zhang, P. Y. Su, X. Q. Lü, J. R. Song, D. D. Fan, W.-K. Wong, R. A. Jones and C.-Y. Su, *Eur. J. Inorg. Chem.*, 2014, 2839.

17 W. X. Feng, Y. Zhang, Z. Zhang, P. Y. Su, X. Q. Lü, J. R. Song, D. D. Fan, W.-K. Wong, R. A. Jones and C. Y. Su, *J. Mater. Chem. C*, 2014, **2**, 1489.

18 S. Comby and J.-C. G. Bünzli, in *Handbook on the Physics and Chemistry of Rare Earths*, ed. K. A. Gschneidner Jr., J.-C. G. Bünzli and V. K. Pecharsky, Elsevier Science B. V., Amsterdam, The Netherlands, 2007, vol. 37, ch. 235.

19 (*a*) C. de Mello Donegá, S. Alves and G. F. De Sá Jr., *Chem. Commun.*, 1996, 1199; (*b*) J. C. de Mello, H. F. Wittmann and R. H. Friend, *Adv. Mater.*, 1997, **9**, 230.

20 G. M. Sheldrick, *SHELXL-97: Program for crystal structure refinement*, Göttingen, Germany, 1997.

21 G. M. Sheldrick, *SADABS*, University of Göttingen, Germany, 1996.

22 W. A. Braunecker and K. Matyjaszewski, *Prog. Polym. Sci.*, 2007, **32**, 93.

23 X. P. Yang, R. A. Jones, M. M. Oye, M. J. Wiester and R. J. Lai, *New J. Chem.*, 2011, **35**, 310.

24 X. P. Yang, R. A. Jones, M. J. Wiester, M. M. Oye and W.-K. Wong, *Cryst. Growth Des.*, 2010, **10**, 970.

25 W. T. Carnall, P. R. Fields and K. Rajnak, *J. Chem. Phys.*, 1968, **49**, 4443.

26 F. J. Steemers, W. Verboom, D. N. Reinhoudt, E. B. van der Tol and J. W. Verhoeven, *J. Am. Chem. Soc.*, 1995, **117**, 9408.

27 M. Latva, H. Takalo, V. M. Mukkala, C. Matachescu, J. C. Rodriguez-Ubis and J. Kanakare, *J. Lumin.*, 1997, **75**, 149.

28 L. J. Xu, G. T. Xu and Z. N. Chen, *Coord. Chem. Rev.*, 2014, **273–274**, 47.

29 (*a*) K. Lunstroot, K. Driesen, P. Nockemann, L. Viau, P. H. Mutin, A. Viouxb and L. Binnemans, *Phys. Chem. Chem. Phys.*, 2010, **12**, 1879; (*b*) W. Q. Fan, J. Feng, S. Y. Song, Y. Q. Lei, G. L. Zheng and H. J. Zhang, *Chem. – Eur. J.*, 2010, **16**, 1903; (*c*) S. Sivakumar and M. L. P. Reddy, *J. Mater. Chem.*, 2012, **22**, 10852; (*d*) S. Biju, Y. K. Eom, J.-C. G. Bünzli and H. K. Kim, *J. Mater. Chem. C*, 2013, **1**, 6935.

30 S. Inoue, T. Kumagai, H. Tamezawa, H. Aota, A. Matsumoto, K. Yokoyama, Y. Matoba and M. Shibano, *J. Polym. Sci., Part A: Polym. Chem.*, 2011, **49**, 156.

31 W. J. Sommer and M. Weck, *Coord. Chem. Rev.*, 2007, **151**, 860.

32 S. K. Yang, A. V. Ambade and M. Weck, *Chem. Soc. Rev.*, 2011, **40**, 129.

33 M. O. Wolf, *Adv. Mater.*, 2001, **13**, 545.

34 P. Gumbley, D. Koylu and S. W. Thomas, *Macromolecules*, 2011, **44**, 7956.

35 F. Mercier, C. Alliot, L. Bion, N. Thromat and P. Toulhoat, *J. Electron Spectrosc. Relat. Phenom.*, 2006, **150**, 21.

36 H. X. Huang, J. Liu and Y. Q. Cai, *J. Lumin.*, 2013, **143**, 447.

37 J. Feng, J. B. Yu, S. Y. Song, L. N. Sun, W. Q. Fan, X. M. Guo, S. Dang and H. J. Zhang, *Dalton Trans.*, 2009, 2406.

38 P. Martin-Ramos, V. Lavín, M. Ramos Silva, I. R. Martín, F. Lahoz, P. Chamorro-Posada, J. A. Paixão and J. Martín-Gil, *J. Mater. Chem. C*, 2013, **1**, 5701.

39 L. D. Carlos, R. A. S. Ferreira, V. e Z. Bermudez, B. Julian-Lopez and P. Escribano, *Chem. Soc. Rev.*, 2011, **40**, 536.